Open access • Journal Article • DOI:10.1088/0004-637X/708/1/834

An extremely top-heavy initial mass function in the galactic center stellar disks

H. Bartko, Fabrice Martins, Sascha Trippe, Tobias K. Fritz ...+18 more authors

Institutions: Max Planck Society, University of Paris, Weizmann Institute of Science, Leiden University ...+3 more institutions

Published on: 01 Jan 2010 - The Astrophysical Journal (IOP Publishing)

Topics: Initial mass function, Stellar mass, Stellar collision, Star formation and O-type star

An extremely top-heavy initial mass function in the galactic center stellar disks

Bartko, M.; Martins, F.; Trippe, S.; Fritz, T.K.; Genzel, R.; Ottl, T.; ... ; Sternberg, A.

The Astrophysical Journal, 708:834–840, 2010 January 1 doi:10.1088/0004-637X/708/1/834

AN EXTREMELY TOP-HEAVY INITIAL MASS FUNCTION IN THE GALACTIC CENTER STELLAR DISKS*

H. Bartko[1], F. Martins[1,2], S. Trippe[3], T. K. Fritz[1], R. Genzel[1,4], T. Ott[1], F. Eisenhauer[1], S. Gillessen[1], T. Paumard[5], T. Alexander[6], K. Dodds-Eden[1], O. Gerhard[1], Y. Levin[7], L. Mascetti[1], S. Nayakshin[8], H. B. Perets[6], G. Perrin[5], O. Pfuhl[1], M. J. Reid[9], D. Rouan[5], M. Zilka[10], and A. Sternberg[10]
[1] Max-Planck-Institute for Extraterrestrial Physics, Garching, Germany; hbartko@mpe.mpg.de, fabrice.martins@graal.univ-montp2.fr
[2] GRAAL-CNRS, Université Montpelier II-UMR5024, Place Eugène Bataillon, F-34095, Montpellier, France
[3] IRAM Grenoble, 300 rue de la piscine, F-38406 Saint Martin d'Heres, France
[4] Department of Physics, University of California, Berkeley, USA
[5] LESIA, Observatoire de Paris, CNRS, UPMC, Université Paris Direrot, Meudon, France
[6] Faculty of Physics, Weizmann Institute of Science, Rehovot 76100, Israel
[7] Leiden University, Leiden Observatory and Lorentz Institute, NL-2300 RA Leiden, The Netherlands
[8] Department of Physics & Astronomy, University of Leicester, Leicester, UK
[9] Harvard-Smithsonian Center for Astrophysics, 60 Garden Street, Cambridge, USA
[10] School of Physics and Astronomy, Tel Aviv University, Tel Aviv 69978, Israel
Received 2009 August 15; accepted 2009 November 13; published 2009 December 15

ABSTRACT

We present new observations of the nuclear star cluster in the central parsec of the Galaxy with the adaptive optics assisted, integral field spectrograph SINFONI on the ESO/VLT. Our work allows the spectroscopic detection of early- and late-type stars to $m_K \geqslant 16$, more than 2 mag deeper than our previous data sets. Our observations result in a total sample of 177 bona fide early-type stars. We find that most of these Wolf Rayet (WR), O-, and B-stars reside in two strongly warped disks between 0.″8 and 12″ from Sgr A*, as well as a central compact concentration (the S-star cluster) centered on Sgr A*. The later type B-stars ($m_K > 15$) in the radial interval between 0.″8 and 12″ seem to be in a more isotropic distribution outside the disks. The observed dearth of late-type stars in the central few arcseconds is puzzling, even when allowing for stellar collisions. The stellar mass function of the disk stars is extremely top heavy with a best-fit power law of $dN/dm \propto m^{-0.45\pm0.3}$. WR/O-stars were formed in situ in a single star formation event ∼6 Myr ago, this mass function probably reflects the initial mass function (IMF). The mass functions of the S-stars inside 0.″8 and of the early-type stars at distances beyond 12″ are compatible with a standard Salpeter/Kroupa IMF (best-fit power law of $dN/dm \propto m^{-2.15\pm0.3}$).

Key words: Galaxy: center – stars: early-type – stars: luminosity function, mass function

Online-only material: color figures

1. INTRODUCTION

The central parsec of the Galaxy harbors more than 100 young massive stars (Forrest et al. 1987; Allen et al. 1990; Krabbe et al. 1995, 1991; Najarro et al. 1997, 1994; Blum et al. 1995; Tamblyn et al. 1996; Genzel et al. 2003; Ghez et al. 2003; Paumard et al. 2006; Martins et al. 2007). This is highly surprising since the tidal forces from the central four million solar mass black hole should make formation of stars by gravitational collapse from a cold interstellar cloud very difficult if not impossible (Morris 1993). Observations have established that most of the Wolf Rayet (WR) stars and O-stars (dwarfs, giants, and supergiants) dominating the luminosity of the early-type population were formed in a well-defined single event ∼6 Myr ago, perhaps as a result of the infall of a gas cloud followed by an in situ star formation event (Krabbe et al. 1995; Paumard et al. 2006). About half of these WR/O-stars between 0.″8 and 12″ from Sgr A* appear to reside in a well defined but highly warped disk that rotates clockwise on the sky (Levin & Beloborodov 2003; Genzel et al. 2003; Paumard et al. 2006; Lu et al. 2009; Bartko et al. 2009). It is less clear how the other half is distributed. Paumard et al. (2006) and Bartko et al. (2009) find evidence for a counterclockwise structure, perhaps a second disk in a dissolving state. Lu et al. (2009) confirm the first stellar disk but do not observe a significant number of stars in the second disk. Within about 1″ of Sgr A* there is a sharp cutoff in the density of WR/O-stars. Instead there is a concentration of fainter stars with randomly oriented and eccentric orbits: the so-called S-star cluster' (Eisenhauer et al. 2005; Gillessen et al. 2009). The brighter members of this central cusp are spectroscopically identified as main-sequence B-stars (Ghez et al. 2003; Eisenhauer et al. 2005; Martins et al. 2008; Gillessen et al. 2009). It is currently debated whether the S-stars formed in the disk(s) and subsequently migrated to the central arcsecond (Levin 2007; Löckmann et al. 2008), or whether they formed outside the central few parsecs, were injected into near-parabolic orbits by massive perturbers and were then captured by the massive black hole (e.g. Hills 1988; Perets et al. 2007).

If star formation indeed has taken place in the vicinity of the massive black hole, it is of great interest to explore the stellar mass function and spatial distribution to gain a better understanding of the processes involved in overcoming the tidal barrier. Likewise it is important to observationally constrain the characteristics and origin of the central S-star cluster. In the following, we present the results of an extensive imaging spectroscopy survey of the central parsec with the adaptive optics (AO) assisted integral field spectrograph SINFONI on the ESO/VLT. We report new observations aimed at defining the spatial distribution and dynamics of the nuclear stars up to $m_K \geqslant 16$ throughout this region and combine this new work with our earlier results on the WR/O-stars and the central S-star cluster.

* Based on observations collected at the ESO Very Large Telescope (programs 075.B-0547, 076.B-0259, and 077.B-0503).

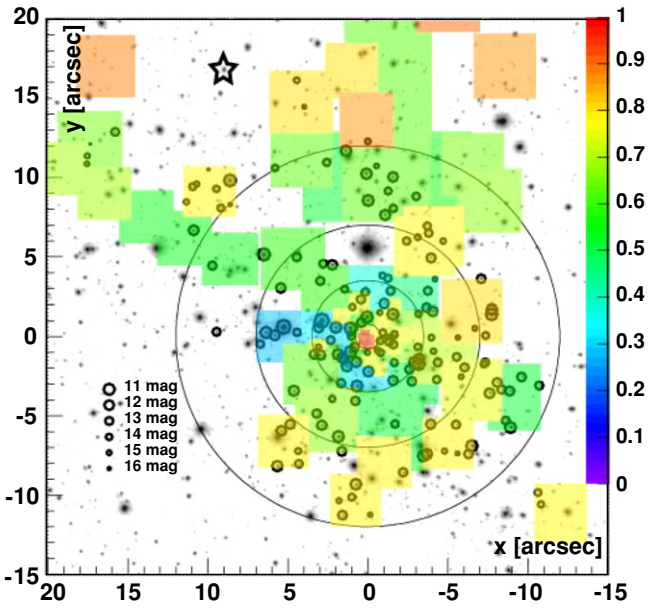

Figure 1. Black circles indicate the sample of early-type stars with $0\farcs8 \leqslant R \leqslant 25''$. The size of the circle scales with the *K*-band magnitude. The large black circles show projected distances of $0\farcs8$, $3\farcs5$, $7''$, and $12''$ from Sgr A*. The colored squares indicate the exposed fields with SINFONI in the 25 mas pixel^{-1} and 100 mas pixel^{-1} scale. The color scale indicates the combined photometric and spectroscopic completeness for an $m_K = 14$ main-sequence early-type star in the observed field. The whole inner $\sim 12''$ region is contained in lower resolution (250 mas pixel^{-1} scale) SINFONI observations (Paumard et al. 2006). The asterisk indicates the visible AO guide star.

(A color version of this figure is available in the online journal.)

2. OBSERVATIONS AND DATA REDUCTION

Observations of the imaging survey were carried out from 2005 to 2009 with SINFONI (Eisenhauer et al. 2003) on the ESO/VLT, partly using natural guide star AO and partly exploiting the laser guide star facility (Rabien et al. 2003; Bonaccini Calia et al. 2006). We covered a total surface area of 15 square arcsec at projected distances below $4''$ from Sgr A* with the AO scale (12.5×25 mas pixel^{-1} scale) resulting in a final *K*-band full width at half maximum (FWHM) of typically about 100 mas. In addition, we observed a total surface area of more than 500 square arcsec with the 50×100 mas pixel^{-1} scale resulting in typical *K*-band FWHMs of about 200 mas. The location of the observed fields (typical integration time per field 2 hr) is indicated in Figure 1. We reduced the data with the software SPRED as in Eisenhauer et al. (2005) and Paumard et al. (2006). Our primary goal in this project is to determine the spatial distribution and dynamics of the early-type stars as a function of their *K*-band magnitude/mass. For this purpose, we need to distinguish from the spectroscopic data early-type stars from late-type stars and to isolate the central star cluster from fore- and background stars.

Late-type stars in the observed magnitude range are giants later than K0III and cool red supergiants. These stars show characteristic CO band head absorption features, which can efficiently be used to remove these stars from our sample. Only three red supergiants have been observed in the central pc of the Galaxy (Blum et al. 2003; Paumard et al. 2006), most notably IRS 7 at an angular distance of $5\farcs5$ from Sgr A*. In contrast to the giants later than K0III, the red supergiants are young and massive stars with ages between 7 and a few tens of megayears (Blum et al. 1996a).

We classified stars as "CO" (late-type) or "non CO" (early-type) depending on the presence or the absence of the CO 2.29 μm $v = 0$–2 band heads (see also Maness et al. 2007). By adding artificial late-type stars to our data, we determined the average efficiency of the CO detection to be better than 98% at $m_K = 16.5$. In order to rate a "non-CO" as bona fide early-type star, we require the detection of at least one of the Brγ He I 2.058 μm or He I 2.112 μm lines at a signal to noise level, which allows a radial velocity measurement with a maximum uncertainty of 100 km s^{-1}. The sample of bona fide early-type stars is essentially free from late-type star interlopers.

Fore- and background early-type stars do not add any significant contamination to the observed population of early-type stars in the central parsec around Sgr A*. Due to the large extinction toward the Galactic Center of $A_K = 2.8$ (see, e.g., Schödel et al. 2007), foreground sources can efficiently be rejected by their very blue $H-K$ band colors. There are only two bright infrared detectable foreground stars (Biretta et al. 1982). Background sources are subject to an even higher extinction and very red $H-K$ band colors. The cusp of early-type stars around Sgr A* is very steep (see Figure 2): $\Sigma(R) \propto R^{-1.4\pm0.2}$. For a cluster in equilibrium the distribution of the line-of-sight distances to Sgr A* is related to the star surface number density distribution (Alexander 2005). Out of the 136 early-type stars in the interval of projected distances $0\farcs8 \leqslant R \leqslant 12''$ only 8/3 stars may have line-of-sight distances larger than 1/2 pc.

We corrected the observed *K*-band magnitude $m_{K,\mathrm{obs}}$ (for the absolute magnitude scale calibration see Blum et al. 1996b; Maness et al. 2007) of the stars for the variation of extinction over the Galactic center region. We calculated the extinction for each position in the Galactic center field, $A_{K,\mathrm{obs}}$, by using the observed *H*-band and *K*-band magnitudes of the 20 nearest neighboring stars, assuming realistic intrinsic colors for the stars and assuming the extinction law from Rieke & Rieke (1989), $A(\lambda) \propto \lambda^{-1.75}$. All magnitudes m_K mentioned below are referred back to a common standard extinction of 2.8: $m_K = m_{K,\mathrm{obs}} + 2.8 - A_{K,\mathrm{obs}}$.

Our total data set contains 177 bona fide early-type stars at projected distances up to $25''$ from Sgr A*. Figure 1 shows the location of the bona fide early-type stars with $R > 0\farcs8$. Of the 177 bona fide early-type stars in our survey, 118 are WR/O-stars and 59 are B-dwarfs ($m_K \geqslant 14.$); 28 WR/O-stars and 34 B-dwarfs are reported here for the first time.

3. NUMBER COUNTS AND COMPLETENESS CORRECTIONS

To study the radial surface density and *K*-band luminosity function (KLF) of the early-type stars, we correct the number of observed stars for both photometric and spectroscopic incompleteness, as well as (for radial surface density plots) for incomplete areal coverage.

The photometric completeness ϵ_{phot} is defined as the probability of detecting a star with a given magnitude in the image generated by integrating over the spectral information of the SINFONI data. For this purpose, we added artificial stars to the spectrally integrated SINFONI images, and determined the probability of re-detecting the artificial stars with an automatic star detection algorithm (Stetson 1987). We used a dense sampling of the image area with a satisfying number of trials (about 2000 trials per image and per flux bin, the exact number depending on respective image dimensions) and tested the completeness was in flux bins of $\Delta m_K = 1$.

The spectroscopic completeness $\epsilon_{\rm spec}$ is the probability of identifying the spectral type of a given, photometrically detected star in a data cube. For this purpose, we added and recovered three-dimensional stellar cubes in analogy with the photometric completeness estimates. These three-dimensional cubes are formed from a spatial point-spread function (PSF) with an early-type star spectrum along the wavelength axis. For each photometrically re-detected star we extracted its spectrum from the data cube and computed a CO index (Maness et al. 2007), which quantifies the relative depth of the CO band head absorption feature. We required a minimum total signal-to-noise ratio of the spectrum in the region of the CO band head of at least 5σ. If the relative depth of the CO band head feature of the artificial early-type star spectrum was smaller than twice the noise, the star was counted as a "spectroscopically re-identified early-type star."

We assign errors to both photometric and spectroscopic completeness values. We confirmed that the completeness values do not change beyond these errors by different settings of the star detection algorithm and the CO index calculation. We computed the combined photometric and spectroscopic completeness as a function of magnitude and location throughout the observed region, propagating the individual errors, to the combined completeness $\epsilon_{\rm comb}(x, y, m_K)$. We calculated completeness maps, which give (as a function of magnitude) the completeness and its error for each observed point. As an example, Figure 1 shows the combined completeness distribution for an $m_K = 14$ main-sequence early-type star. In our survey an average 50% completeness is achieved for an $m_K = 15$ star. The spectroscopy is deeper toward the central S-star cluster and several fields without bright stars (Figure 1).

We derived an effective exposed area $A_{\rm eff}(R_1, R_2, m_K)$ (including error) over an annulus between R_1 and R_2 around Sgr A* as a function of m_K taking the SINFONI exposure locations and the completeness values including their errors into account:

$$A_{\rm eff}(R_1, R_2, m_K) = \int_{\sqrt{x^2+y^2}\geqslant R_1}^{\sqrt{x^2+y^2}\leqslant R_2} \epsilon_{\rm comb}(x, y, m_K) dx dy \ . \quad (1)$$

Finally, we computed from the number of observed stars $N_{\rm stars,obs.}(R_1, R_2, m_K)$ in an annulus between R_1 and R_2 around Sgr A* the K-band luminosity function KLF(R_1, R_2, m_K) and the surface density $\Sigma(R_1, R_2)$:

$$\mathrm{KLF}(R_1, R_2, m_K) = \frac{N_{\rm stars,\,obs.}(R_1, R_2, m_K)}{A_{\rm eff}(R_1, R_2, m_K)}$$

$$\Sigma(R_1, R_2) = \sum_{m_K} \frac{N_{\rm stars,\,obs.}(R_1, R_2, m_K)}{A_{\rm eff}(R_1, R_2, m_K)} \ .$$

4. RESULTS

4.1. Surface Density Profiles

Figure 2 shows the projected-, completeness-, and coverage-corrected surface density profiles for all stars with $m_K < 17$, late-type stars with $m_K < 15.5$, the WR/O-stars ($m_K < 14$), and B-dwarfs in the magnitude interval $14.5 \leqslant m_K \leqslant 15.5$. The radial surface density of the clockwise WR/O-stars follows a power law $\Sigma(R) \propto R^{-1.4\pm0.2}$ between 0.″8 and 15″. Extrapolating this power law to smaller projected distances yields 28 ± 8 clockwise WR/O-stars for $R < 0.''8$. At the 95% confidence level we expect more than 12 stars within 0.″8. We did not observe any WR/O-star in this region. The Poisson probability

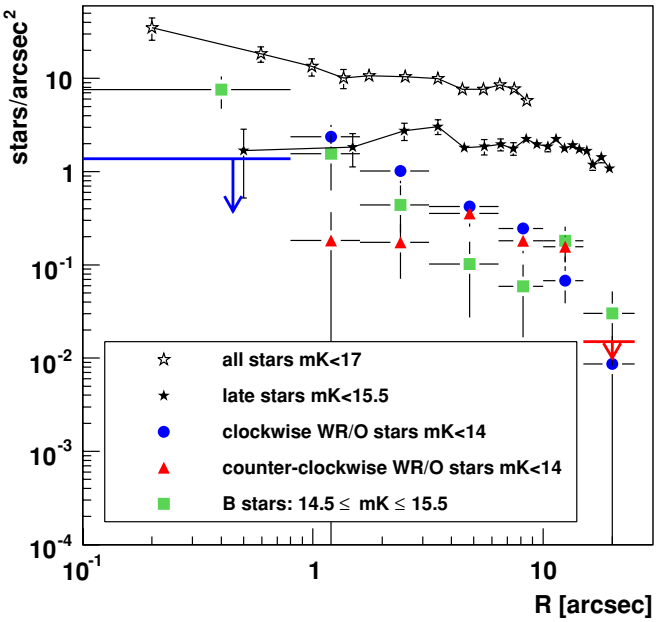

Figure 2. Projected-, completeness-, and coverage-corrected surface density as a function of distance to Sgr A*. Blue points (red triangles) indicate WR/O ($m_K < 14$) stars on clockwise (counterclockwise) orbits and green squares indicate B-dwarfs in the magnitude bin $14.5 \leqslant m_K \leqslant 15.5$. The blue and red arrows show the 90% confidence limit to the number density of WR/O-stars in the innermost 0.″8 and counterclockwise WR/O-stars in the radial interval between 15″ and 25″. For comparison, the open asterisks indicate all stars with $m_K < 17$ and the full asterisks the identified late-type stars with $m_K < 15.5$.

(A color version of this figure is available in the online journal.)

to observe no star for 28 expected stars is 5.6×10^{-13} and the Poisson probability to observe none of 12 expected stars is still 6×10^{-6}. Therefore we conclude that there is a significant cutoff in the distribution of WR/O-stars at $R = 0.''8$. The difference compared to the R^{-2} power law suggested by earlier work (Paumard et al. 2006; Lu et al. 2009; Bartko et al. 2009) is due to the thorough completeness and coverage correction applied here. The surface density distribution of the counterclockwise WR/O-stars is rather flat between 0.″8 and 15″, mainly because it has a larger central "hole" than the clockwise stars and a maximum in the distribution at around 4.″5. The radial surface density profile of B-dwarfs in the magnitude interval $14.5 \leqslant m_K \leqslant 15.5$ drops smoothly from the central 0.″8, where the S-stars reside, out to about 25″. Its distribution is similar to the clockwise WR/O-stars with a best-fitting power law of $\Sigma(R) \propto R^{-1.5 \pm 0.2}$. In strong contrast to the early-type stars, late-type stars with $m_K \leqslant 15.5$ exhibit a flat distribution inside of 10″, in excellent agreement with Buchholz et al. (2009) and Do et al. (2009).

4.2. K-Band Luminosity Function

Figure 3 shows the completeness-corrected K-band luminosity functions of early-type stars in three radial intervals $R < 0.''8$, $0.''8 \leqslant R \leqslant 12''$, and $12'' < R < 25''$. The slope of the KLF is sensitive to the stellar mass function (MF). If the population formed in situ without being affected by dynamical effects that might alter the mix of stellar masses in the observed sample, the observed KLF of a young population is directly related to the initial stellar mass function (IMF).

The stellar disks (best defined in the radial interval $0.''8 \leqslant R \leqslant 12''$, see Figure 2) and the randomly orbiting S-stars (in the radial interval $R < 0.''8$) are dynamically distinct. The S-stars

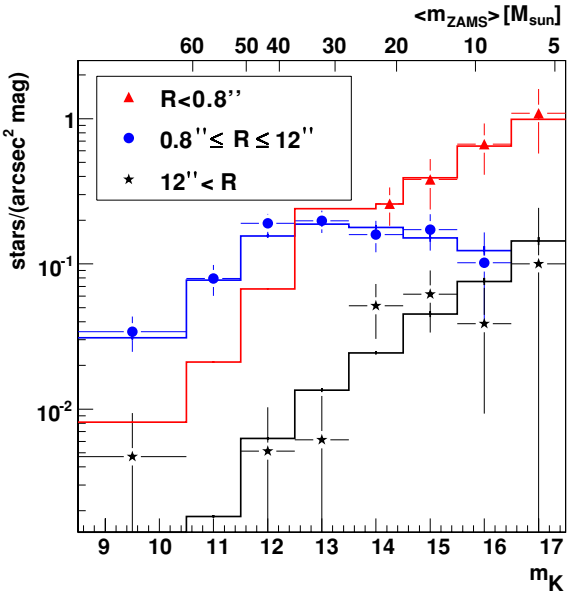

Figure 3. Completeness-corrected K-band luminosity functions of early-type stars in three radial intervals $R < 0.''8$ (red triangles, scaled by a factor 0.05), $0.''8 \leqslant R \leqslant 12''$ (blue points), and $12'' < R < 25''$ (black asterisks). For a 6 Myr population the best-fitting IMF in the radial interval $0.''8 \leqslant R \leqslant 12''$, where the disks of early-type stars are most prominent, is extremely top heavy and clearly different from the IMFs of the S-stars and the field stars beyond $12''$. It can be fitted by a power-law IMF of $dN/dm \propto m^{-0.45 \pm 0.3}$ or the IMF proposed by Bonnell & Rice (2008). The IMF of the field stars beyond $12''$ as well as the S-stars within $0.''8$ can be fitted by a power-law IMF of $dN/dm \propto m^{-2.15 \pm 0.3}$, consistent with a standard Salpeter/Kroupa IMF. These latter KLFs can also be fitted by somewhat older populations with a continuous star formation history, which would then, however, predict lower numbers of $m_K \leqslant 14$ stars (relevant for S-star cluster). The top x-axis shows the average initial mass of the early-type stars contributing to the K-band magnitude bins for the case of a starburst 6 Myr ago with an IMF with a slope of $dN/dm \propto m^{-0.45 \pm 0.3}$ as generated with the STARS code. Most of the stars with $m_K > 14$ are B dwarfs, the brighter magnitude bins contain O dwarfs, giants, and WR stars. The main sequence ends at about $m_K = 12$, corresponding to an initial stellar mass of about 25 $M_\odot$.

(A color version of this figure is available in the online journal.)

have a different formation process than the stellar disks (Perets et al. 2009).

The two main scenarios discussed in the literature for the origin of the disk-like structures of young stars in the Galactic Center (GC) are the *infalling cluster* model (Gerhard 2001; McMillan & Portegies Zwart 2003; Portegies Zwart et al. 2003; Kim & Morris 2003; Kim et al. 2004; Gürkan & Rasio 2005) and the in situ star formation model (Levin & Beloborodov 2003; Genzel et al. 2003; Goodman 2003; Milosavljević & Loeb 2004; Nayakshin & Cuadra 2005; Paumard et al. 2006; Klessen et al. 2007; Bonnell & Rice 2008; Mapelli et al 2008; Hobbs & Nayakshin 2009).

In the *infalling cluster* scenario, a cluster of young stars formed at a distance of at least a few parsecs from the GC and then spiraled inward by dynamical friction. As it finally enters the central parsec it is tidally disrupted and forms a disk-like configuration. If the cluster is dense enough to undergo significant internal mass segregation during the in-spiral phase this scenario does predict a fairly flat MF for the innermost deposited stars even if the assumed intrinsic IMF of the cluster is a standard one (MF: $dN/dm \propto m^{-1.1}$, Gürkan & Rasio 2005). This is because mass segregation within the cluster leads to a differential shedding of stars of different masses as the cluster is tidally stripped during in-spiral. Lower mass stars are deposited further out, while the most massive stars sink the farthest in, especially if the cluster contains a central intermediate mass black hole (Gürkan & Rasio 2005). The differential shedding of different stellar masses combined with the predicted flat surface density of the deposited cluster stars ($\Sigma \propto R^{-0.75}$; Berukoff & Hansen 2006) would then lead to a strong radial change in the MF and a large "sea" of B-stars outside the region where most of the O/WR-stars are located in the plane of the stellar disks. No such gradient is observed in the main part of the disk ($R < 12''$). Figure 3 does show that the KLF and MF of the stars outside $12''$ steepens, consistent with a normal IMF. The observed B-stars at $R > 12''$, however, have large angular offsets to the disk angular momentum directions and are compatible with isotropic orbits, indicating that these stars were not formed in the same way as the disk stars. In addition, the steep surface density distribution excludes that there are enough B-stars at large distances to make up for the shortage of such stars in the central $12''$: 49.3 ± 5.7 stars in the magnitude range $13.5 \leqslant m_K \leqslant 16.5$ would be needed (assuming a standard Salpeter/Kroupa IMF) in the radial interval $12'' \leqslant R \leqslant 25''$, but only 13 stars have been observed.

In the in situ model, a clump or clumps of gas fall into the GC, where they form a disk-like structure. The gaseous disk then fragments to form stars. The detailed observations by Paumard et al. (2006), Bartko et al. (2009), and Lu et al. (2009) are compatible with an in situ formation of these WR/O-stars in a clockwise rotating disk and another highly inclined counterclockwise structure, possibly a disk. The mass segregation timescales in the GC are much larger than 6 Myr (Alexander 2005). We therefore assume that the stars generated in situ in the starburst 6 Myr ago are almost fully contained in the observed sample of early-type stars in the radial interval $0.''8 \leqslant R \leqslant 12''$.

Our observations clearly demonstrate that the (I)MF in the radial interval $0.''8 \leqslant R \leqslant 12''$, where the disks of early-type stars are most prominent (see Figure 2), must be extremely top heavy. This MF is also clearly different from the MFs of the S-star cluster and from the region outside $12''$.

The histograms in Figure 3 show three theoretical model luminosity functions with different IMFs (see, e.g., Muench et al. 2000, 2002). We computed these models using the population synthesis code STARS (Sternberg 1998; Sternberg et al. 2003) assuming solar metallicity Geneva tracks, for a cluster age of 6 Myr, and an exponentially decaying star burst with a $1/e$ timescale of 1 Myr. This is the best-fitting age and duration of a single star formation event derived from the Hertzsprung–Russell diagram distribution of the O/B-stars and the ratios of various sub-types of WR-stars (Paumard et al. 2006). STARS computes K magnitudes using empirical Schmidt–Kaler bolometric corrections and $V-K$ colors for dwarfs, giants, and supergiants. The predicted fractions of O/B main-sequence stars and giants as well as WR stars agree well with the observations (Paumard et al. 2006): stars with $m_K < 12$ are WR stars and stars with $m_K > 15$ are B main-sequence stars. Stars with $m_K \sim 13$ are WR stars (66%), evolved early B-stars (31%) and late O-stars (3%). Stars with $m_K \sim 14$ are O-stars (15%) and evolved early B-stars (85%). Martins et al. (2007) presented detailed stellar atmosphere modelings of a significant fraction of the post-main-sequence blue supergiants and WR stars, which have ages of 4–8 Myr and zero-age main-sequence (ZAMS) masses of at least 60 $M_\odot$, see also Ott et al. (1999) and Martins et al. (2006). The average properties of the generated stars are compatible with the observations.

The KLF in the radial interval $0.''8 \leqslant R \leqslant 12''$ can be fitted by a power-law IMF of $dN/dm \propto m^{-0.45 \pm 0.3}$ ($\chi^2 = 4.6$ for

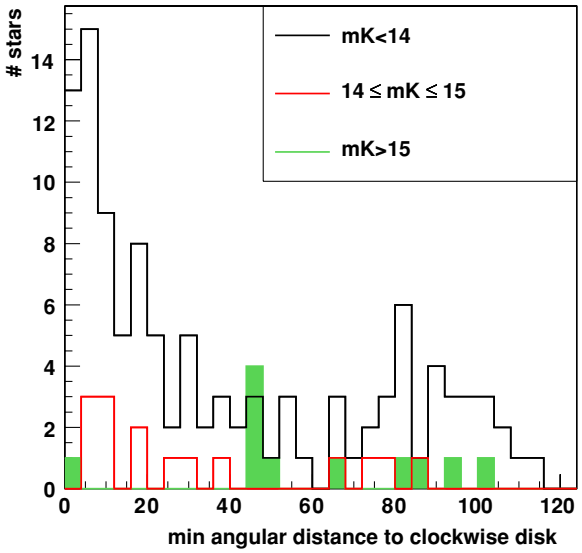

Figure 4. Distribution of the reconstructed angular differences from the local average angular momentum direction of the clockwise system for the early-type stars with projected distances between 0.″8 and 12″. The three distributions correspond to different *K*-band luminosities: black, $m_K < 14$; red, $14 \leqslant m_K \leqslant 15$; green, $mK > 15$. Only 1 out of 11 stars fainter than $m_K = 15$ is compatible with the clockwise disk.

(A color version of this figure is available in the online journal.)

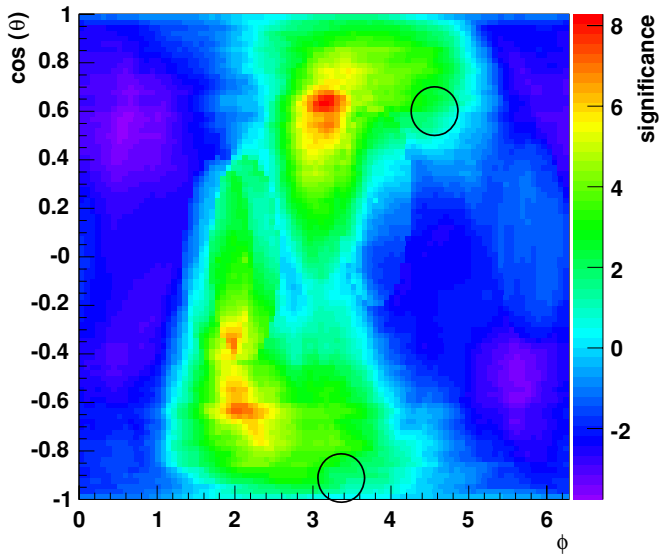

Figure 5. Cylindrical equal area projection of the distribution of significance in the sky (25° aperture, see Bartko et al. 2009) for 82 bona fide early-type stars ($m_K < 14$) with projected distances between 3.″5 and 15″. The disk positions of Paumard et al. (2006) are marked with full black circles. There are two extended excesses visible for clockwise and counterclockwise stars, with maximum significances of 8.2σ and 7.1σ, respectively. We attribute these two extended excess systems as two warped systems of stars.

(A color version of this figure is available in the online journal.)

6 degrees of freedom). For comparison, the standard Salpeter/Kroupa IMF has a high-mass power law of $dN/dm \propto m^{-2.3}$. The IMF found by Bonnell & Rice (2008) for their $10^5\ M_\odot$ cloud simulation also gives a reasonable fit to the data ($\chi^2 = 7.6$, 6 degrees of freedom). We have also selected only those early-type stars, which have an angular offset of less than 10° from the local disk angular momentum direction (see Bartko et al. 2009) and subsequently fitted by the theoretical KLF as a function of IMF slope. The obtained IMF slope agrees with the IMF slope of all stars in the radial interval $0.''8 \leqslant R \leqslant 12''$ within errors.

The IMF of the field early-type stars beyond 12″ and the S-stars within 0.″8 can be fitted by a power-law IMF with a slope of $dN/dm \propto m^{-2.15 \pm 0.3}$, compatible with a standard Salpeter/Kroupa IMF. These latter KLFs can also be fitted by Salpeter/Kroupa IMFs and continuous star formation histories with moderate ages (⩽60 Myr).

It is straightforward to compute a one-to-one relation between observed *K*-band magnitude and initial mass for stars on the main sequence. However, for evolved stars a range of masses contribute at a given *K* magnitude. Therefore, we do not estimate the initial mass for each star but rather compare the observed distribution of *K*-band magnitudes to the simulated magnitude distribution for different IMFs. The top *x*-axis of Figure 3 shows the average initial mass of the early-type stars contributing to the *K*-band magnitude bins for a 6 Myr old cluster for an IMF of $dN/dm \propto m^{-0.45}$ as generated with the STARS code. Most of the stars with $m_K > 14$ are B dwarfs, the brighter magnitude bins contain O dwarfs, giants, and WR stars. The main sequence ends at about $m_K = 12$, corresponding to stars with initial masses of about $25\ M_\odot$ with main-sequence lifetimes of 6 Myr.

An $m_K = 16.5$ early-type star for a 6 Myr old population corresponds approximately to a B5V main-sequence star with a ZAMS mass of about $7\ M_\odot$ (see Figure 3). The most massive stars with an individual mass estimates have ZAMS masses of at least $60\ M_\odot$ (Martins et al. 2006, 2007). Our estimated IMF slope of the stellar disks ($dN/dm \propto m^{-0.45 \pm 0.3}$) is therefore at least valid over the mass interval 7–60 $M_\odot$.

4.3. Orbital Angular Momentum Directions

Figure 4 shows the distributions of the reconstructed angular differences from the local average angular momentum direction of the clockwise system, as defined in Bartko et al. (2009), for the early-type stars with projected distances between 0.″8 and 12″. The three distributions correspond to different *K*-band luminosities: $m_K < 14$, $14 \leqslant m_K \leqslant 15$, and $m_K > 15$. The peak at small angles corresponds to the clockwise system: 50 out of 110 stars with $m_K < 14$ have offsets below 20° and 8 out of 15 stars with $14 \leqslant m_K \leqslant 15$ have offsets below 20°. In contrast, only 1 out of 11 stars fainter than $m_K = 15$ is compatible with the clockwise disk. This may be an indication that most of the few later B-dwarfs observed in the region of the disks do not belong to the clockwise system but rather to the background population seen at projected distances beyond 12″, which has a more standard IMF.

According to Figure 2, the clockwise system of massive early-type stars is best defined in the radial range between 0.″8 and 10″ and has a steep surface density distribution. However, most of the counterclockwise stars reside in the range between 3.″5 and 15″, where we have added considerable SINFONI sky coverage compared to the study of Bartko et al. (2009). In order to test for the existence of a significant system of counterclockwise stars, we have computed a sky significance map of angular momentum overdensities for all bona fide early-type stars ($m_K < 14$) with projected distances between 3.″5 and 15″, see Figure 5. For the technical details see Bartko et al. (2009). There are two extended excesses visible for clockwise and counterclockwise stars, with maximum significances of 8.2σ and 7.1σ, respectively. These maximum excesses are clearly offset from the positions found at small projected distances (Paumard et al. 2006; Lu et al. 2009; Bartko et al. 2009) indicating that the two extended excess systems are most probably two warped systems of stars. We confirm a significant counterclockwise system of stars.

5. DISCUSSION

The observations discussed in the last section, in combination with the results presented in recent published work (Genzel et al. 2003; Eisenhauer et al. 2005; Nayakshin & Sunyaev 2005; Schödel et al. 2007; Paumard et al. 2006; Lu et al. 2009; Bartko et al. 2009; Gillessen et al. 2009; Buchholz et al. 2009; Do et al. 2009), yield the following complex and rather unexpected properties of the stellar cluster surrounding the central black hole:

1. Most of the early-type stars in the central parsec reside in a combination of a central concentration of main-sequence B-stars centered on the black hole (the "S-star cluster"), plus two strongly warped and almost orthogonal disks (or planar sets of streamers) of WR-, O-, and early B-stars. One disk is more massive than the second ($\sim 10^4$ and $\sim 5 \times 10^3\ M_\odot$, computed from the completeness- and exposure-corrected number counts and the best-fit IMF). The second disk is less well defined, perhaps because it is more disrupted. The surface density distribution of the B-stars appears to decline smoothly with approximately constant slope (1.5) from the central S-star cluster to the region of the disks. However, both the dynamics and the mass function change abruptly at 1″. Inside this radius, the stellar orbit distribution is random and the ellipticity distribution is close to but somewhat hotter than a thermal distribution (Gillessen et al. 2009). The observed KLF can be well fitted by a "standard" Salpeter/Kroupa IMF for a single age or continuously star forming population of age a few to 60 Myr. Just outside of this region most of the WR/O-stars are in the dominant clockwise disk, which has a 10° opening angle and stellar orbits with modest ($e \sim 0.35$) eccentricities. The IMF is extremely flat (power-law slope 0.45) with a mean stellar mass of $30\ M_\odot$. Outside of the region dominated by the two disks, at $R \geqslant 12''$, the KLF appears to again approach that of a "standard" IMF. Note, however, that even between 1 and $12'' \sim$ 20–30% of the WR/O-stars, and probably a larger fraction of the B-stars, do not appear to belong to either disk system.
2. The late-type stars of all luminosities, from the brightest thermally pulsing asymptotic giant branch stars to the faintest, low-mass red clump stars, do not show a central concentration that might resemble a classical equilibrium stellar "cusp" as predicted by all theoretical studies (Bahcall & Wolf 1976, 1977; Freitag et al. 2006; Hopman & Alexander 2006). The brightest late-type stars show a central hole of radius a few to 7″ (Sellgren et al. 1990; Genzel et al. 1996; Haller et al. 1996) and even the faint early K-giants with $m_K \sim 15$ show a flat core of radius 10″ (Buchholz et al. 2009; Do et al. 2009), see Figure 2. The combination of the S-star cluster (mostly unrelaxed early-type stars) and the flat late-type star distribution "conspire" to give a shallow overall cusp (surface density slope 0.2 . . .0.4) found in the faint star counts in Figure 1 (Genzel et al. 2003; Schödel et al. 2007).

   The observations suggest that the two WR/O/B-star disks between 0.″8 and 12″ are structurally and dynamically distinct from both the S-star cluster and the outer region. The properties of these warped disks (or sets of streamers), including in particular their steep surface density distribution, their top heavy IMF, and their relatively low total stellar masses, all strongly favor an in situ star formation model (Paumard et al. 2006; Lu et al. 2009; Bartko et al. 2009; Berukoff & Hansen 2006) and broadly agree with the findings in recent hydrodynamical simulations (Bonnell & Rice 2008; Hobbs & Nayakshin 2009) of star formation triggered by gas cloud infall. The sharp transition at 0.″8 between disk zone and S-star cluster, both in terms of dynamics and mass function, in our opinion also strongly disfavors migration scenarios from the disks for the origin of the S-star cluster. In turn, this sharp transition supports the "injection and capture" scenarios mentioned in the introduction.

   The large central core (and perhaps even central hole, see Buchholz et al. 2009; Do et al. 2009) in the density distribution of late-type stars of all luminosities is puzzling and currently not understood. There are a number of possible interpretations, none of which at present offer a compelling explanation. As discussed by Do et al. (2009) and Buchholz et al. (2009) equilibrium mass segregation by itself cannot account for this distribution (Freitag et al. 2006; Hopman & Alexander 2006), as even in a multi-mass cluster the lightest stars attain a radial density distribution that is steeper than R^{-1} (probably excluded by the data: Do et al. 2009). Simulations indicate that physical collisions with main-sequence stars and stellar black holes can remove moderately bright giants in the central arcsecond, but not over a much larger region, nor to $m_K \sim 15$ (Dale et al. 2009). Likewise, tidal disruption of stars may play a role near the massive black hole (Perets et al. 2009) but it needs to be investigated whether they are frequent enough to remove the entire old cusp. The in-spiral of an intermediate mass black hole can plausibly gouge out a large enough core in the stellar distribution (Milosavljevic & Merritt 2001; Baumgardt et al. 2006) but there is no evidence for such a second black hole from the dynamical properties of the S-stars or late-type stars, nor from the motion of Sgr A* itself (Gillessen et al. 2009; Gualandris & Merritt 2009; Trippe et al. 2008; Reid & Brunnthaler 2004). Merritt (2009) has pointed out that the two-body relaxation timescale probably is significantly longer than the age of the Galactic center star cluster (and the Hubble time) throughout the central parsec, especially if the spatial distribution of the giants is similar to that of most of the stellar mass. As a result, the observed large core may reflect the initial conditions of the Galactic center nuclear cluster. Trippe et al. (2008) find, however, that the dynamics of the old star cluster is consistent with a relaxed, fully phase mixed system. In addition, Alexander (2007) has pointed out the importance of relaxation processes much faster than the standard two-body rate (including the massive perturbers proposed by Perets et al. 2007). The top-heavy IMF discussed in this paper (if applicable to early star formation episodes) would obviously also lead to a lack of old low mass giants in the core. To explain the flat or even inverted radial slope (Do et al. 2009; Buchholz et al. 2009, this paper), the IMF probably would have to depend strongly on radius. The remarkable properties of the Galactic center nuclear star cluster remain puzzling and continue to give us food for thought and further work.

We thank all the ESO staff for their help during the various observing runs, and Melvyn Davies for a discussion on his work on stellar collisions. We thank the DFG for support via German-Israeli Project Cooperation grant STE1869/1-1.GE625/15-1. We thank the referee, Don Figer, for his comments and suggestions.

REFERENCES

Alexander, T. 2005, Phys. Rev., 419, 65
Alexander, T. 2007, arXiv:0708.0688
Allen, D. A., Hyland, A. R., & Hillier, D. J. 1990, MNRAS, 244, 706
Bahcall, J. N., & Wolf, R. A. 1976, ApJ, 209, 214
Bahcall, J. N., & Wolf, R. A. 1977, ApJ, 216, 883
Bartko, H., et al. 2009, ApJ, 697, 1741
Baumgardt, H., et al. 2006, MNRAS, 372, 467
Berukoff, S. J., & Hansen, B. M. S. 2006, ApJ, 650, 901
Biretta, J. A., Lo, K. Y., & Young, P. J. 1982, ApJ, 262, 578
Blum, R. D., Depoy, D. L., & Sellgren, K. 1995, ApJ, 441, 603
Blum, R. D., Sellgren, K., & Depoy, D. L. 1996a, ApJ, 470, 864
Blum, R. D., Sellgren, K., & Depoy, D. L. 1996b, AJ, 112, 1988
Blum, R. D., Ramirez, S. V., Sellgren, K., & Olsen, K. 2003, ApJ, 597, 323
Bonaccini Calia, D., et al. 2006, Proc. SPIE, 6272, 6
Bonnell, I. A., & Rice, W. K. M. 2008, Science, 321, 1060
Buchholz, R. M., Schödel, R., & Eckart, A. 2009, A&A, 499, 483
Dale, J. E., et al. 2009, MNRAS, 393, 1016
Do, T., et al. 2009, ApJ, 703, 1323
Eisenhauer, F., et al. 2003, Messenger, 113, 17
Eisenhauer, F., et al. 2005, ApJ, 628, 246
Forrest, W. J., et al. 1987, in AIP Conf. Proc. 1555, The Galactic Center, ed. D. C. Backer (Melville, NY: AIP), 153
Freitag, M., Amaro-Seoane, P., & Kalogera, V. 2006, ApJ, 649, 91
Genzel, R., et al. 1996, ApJ, 472, 153
Genzel, R., et al. 2003, ApJ, 594, 812
Gerhard, O. 2001, ApJ, 546, L39
Ghez, A., et al. 2003, ApJ, 586, L127
Gillessen, S., et al. 2009, ApJ, 692, 1075
Goodman, J. 2003, MNRAS, 339, 937
Gualandris, A., & Merritt, D. 2009, ApJ, 705, 361
Gürkan, M. A., & Rasio, F. A. 2005, ApJ, 628, 236
Haller, J. W., et al. 1996, ApJ, 456, 194
Hills, J. G. 1988, Nature, 331, 687
Hobbs, A., & Nayakshin, S. 2009, MNRAS, 394, 191
Hopman, C., & Alexander, T. 2006, ApJ, 645, L133
Kim, S. S., & Morris, M. 2003, ApJ, 597, 312
Kim, S. S., Figer, D. F., & Morris, M. 2004, ApJ, 607, L123
Klessen, R. S., Spaans, M., & Jappsen, A. K. 2007, MNRAS, 374, L29
Krabbe, A., et al. 1991, ApJ, 382, L19
Krabbe, A., et al. 1995, ApJ, 447, L95
Levin, Y., & Beloborodov, A. M. 2003, ApJ, 590, L33
Levin, Y. 2007, MNRAS, 374, 515
Löckmann, U., Baumgardt, H., & Kroupa, P. 2008, ApJ, 683, L151
Lu, J. R., et al. 2009, ApJ, 690, 1463
Maness, H., et al. 2007, ApJ, 669, 1024
Mapelli, M., Hayfield, T., Mayer, L., & Wadsley, J. 2008, arXiv0805.0185
Martins, F., et al. 2006, ApJ, 649, 103
Martins, F., et al. 2007, A&A, 468, 233
Martins, F., et al. 2008, ApJ, 672, 119
McMillan, S. L. W., & Portegies Zwart, S. F. 2003, ApJ, 596, 314
Merritt, D. 2009, arXiv0909.1318
Milosavljevic, M., & Merritt, D. 2001, ApJ, 563, 34
Milosavljević, M., & Loeb, A. 2004, ApJ, 604, L45
Morris, M. 1993, ApJ, 408, 493
Muench, A. A., Lada, E. A., & Lada, C. J. 2000, ApJ, 533, 358
Muench, A. A., et al. 2000, ApJ, 533, 358
Najarro, F., et al. 1994, A&A, 285, 573
Najarro, F., et al. 1997, A&A, 325, 700
Nayakshin, S., & Cuadra, J. J. 2005, A&A, 437, 437
Nayakshin, S., & Sunyaev, R. 2005, MNRAS, 364, L23
Ott, T., Eckart, A., & Genzel, R. 1999, ApJ, 523, 248
Paumard, T., et al. 2006, ApJ, 643, 1011
Perets, H. B., Hopman, C., & Alexander, T. 2007, ApJ, 656, 709
Perets, H. B., et al. 2009, ApJ, 702, 884
Portegies Zwart, S. F., McMillan, S. L. W., & Gerhard, O. 2003, ApJ, 593, 352
Rabien, S., et al. 2003, Proc. SPIE, 4839, 393
Reid, M. J., & Brunnthaler, A. 2004, ApJ, 616, 872
Rieke, G. H., & Rieke, M. J. 1989, ApJ, 344, L5
Schödel, R., et al. 2007, A&A, 469, 125
Sellgren, K., McGinn, M. T., Becklin, E. E., & Hall, D. N. 1990, ApJ, 359, 112
Sternberg, A. 1998, ApJ, 506, 721
Sternberg, A., Hoffmann, T. L., & Pauldrach, A. W. A. 2003, ApJ, 599, 1333
Stetson, P. B. 1987, PASP, 99, 191
Tamblyn, P., et al. 1996, ApJ, 456, 206
Trippe et al. 2008, A&A, 492, 419